Functional Metalloblock Copolymers for the Preparation and *in situ* Functionalization of Porous Silica Films

Nicole Herzog,[†] *Hanna Hübner,*[‡] *Christian Rüttiger,*[†] *Markus Gallei**[‡] *and Annette Andrieu-Brunsen**[†]

AUTHOR ADDRESS.

[†] Ernst-Berl Institut für Technische und Makromolekulare Chemie, Technical University of Darmstadt, Alarich-Weiss-Str. 4, D-64287 Darmstadt, Germany.

‡ Chair in Polymer Chemistry, Saarland University, Campus Saarbrücken C4 2, 66123 Saarbrücken, Germany.

KEYWORDS. metalloblock copolymers, functional template, mesoporous hybrid materials, gating ionic transport

ABSTRACT. Stimuli-responsive mesoporous silica films were prepared by evaporation-induced self-assembly through the physical entrapment of a functional metalloblock copolymer structuring agent, which simultaneously served to functionalize the mesopore. After end-functionalization with a silane group, the applied functional metalloblock copolymers were covalently integrated into the silica mesopore wall. In addition, they were partly degraded after the formation of the mesoporous film which enabled the precise design of accessible mesopores. These polymer–silica hybrid materials exhibited remarkable and gating ionic permselectivity and offer the potential for highly precise pore filling design and combination with high-throughput printing techniques. This *in situ* functionalization strategy of mesoporous silica using responsive metalloblock copolymers has the potential to improve how we approach the design of complex architectures at the nanoscale for tailored transport. This functionalization strategy paves the way for a variety of technologies based on molecular transport in nanoscale pores, including separation, sensing, catalysis, and energy conversion.

INTRODUCTION. Mesoporous silica is of interest for a variety of different technologies because it offers a high thermal stability[1] accompanied by a very large accessible surface.[2, 3] Due to a high concentration of surface species, further functionalization can be easily implemented. Therefore, mesoporous silica hybrid materials have garnered significant attention in biosensing applications or drug release systems, for example. Other applications are catalysis, sensor technology, photocatalysis technology, water filtration or separation and energy storage or conversion.[4-11]

Generally, mesoporous silica is obtained by soft templating using surfactants or block copolymers (BCPs) as structure directing agents. In general, BCPs are capable of self-organization and are excellent materials for the design of tailor-made nanostructures in the bulk state or in selective solvents.[12-14] In the case of soft-templating methods based on BCP self-assembly in combination with silica precursors, the BCPs can be removed by calcination or chemical extraction. As a result, highly ordered and porous inorganic or hybrid materials can be obtained. Therefore, mesoporous films are synthesized by evaporation-induced self-assembly (EISA), which was first investigated by Brinker et al.[15] Since the first scientific report, many different surfactants have been described, and a variety of functional and stimuli-responsive BCPs are known for the formation of (meso)porous materials.[16-23] Currently, a variety of mesoporous films are routinely fabricated using surfactant-templated materials.[22, 24] Surprisingly, the design of BCPs and their intrinsic capability for the formation of highly ordered structures have not been systematically studied for the preparation of functional templates that enables *in situ* functionalization using EISA.

Although EISA produces silica films with tailored micro- and mesostructures, the preparation of functionalized mesoporous materials currently represents a multistep synthesis approach.[25] To synthesize functionalized mesoporous silica films, co-condensation of functional organosilanes during EISA or post-grafting of functional organosilanes is applied – and often – followed by subsequent polymerization strategies.[3, 4, 26] A disadvantage of post-grafting methods is that inhomogeneities for the obtained surfaces may occur.[8] For example, the pore entrance can reveal a higher degree of functionalization than areas that are located in the interior of the pores. On the other hand, functionalization strategies, especially involving small hydrophilic molecules, e.g., aminopropyltriethoxysilane (APTES), have been successfully demonstrated using co-

condensation. As a major drawback of this route, the mesoporous structure is usually affected[3]; also, the introduction of hydrophobic precursor molecules is difficult and limited to relatively low amounts.[8] Upper limit organosilane ratios of up to 40 mol% are reported under ideal conditions.[26] In addition to small molecules, the polymer functionalization of mesopores is of special interest with respect to tailoring mesopore characteristics. A prominent example is the gating of mesopore transport based on functional polymers.[27-30] In this context, grafting from stimuli-responsive polymers has attracted enormous attention in the recent past, resulting in mesopores changing their charge or wettability upon a certain stimulus.

A plethora of stimuli-responsive mesopores have been reported that show transport in response to all well-known triggers, such as temperature, pH, solvent, ions, and light.[30-32] In addition to these classical stimuli, redox-responsive polymers are very interesting due to their ability to simultaneously change the charge and wettability of a mesopore by reacting with an oxidizing or reducing agent or by application of an electric current.[28, 33] Despite the responsive transport characteristics of these polymer functionalized mesopores, these materials were prepared using a multistep grafting-from approach.[34-37]

Because of their excellent redox-active, semiconductive, photophysical, optoelectronic and mechanical properties and for the preparation of advanced (magnetic) ceramics, metal-containing polymers, also referred to as metallopolymers, have attracted significant interest as a platform for novel functional materials.[38-40] In the recent past, metallopolymers containing the ferrocene/ferrocenium redox couple have attracted significant interest due to the unique capability of (electro)chemical switching between hydrophobic ferrocene and comparably hydrophilic

ferrocenium moieties. The functionalization of mesoporous ceramic films or paper with ferrocene-containing polymers induces switching of water imbibition based on changes between wetting states.[28, 41-46] To the best of our knowledge, metalloblock copolymers for the *in situ* functionalization of silica-based mesopores have not been investigated in more detail.

Herein, we report the synthesis of amphiphilic polystyrene-*b*-poly(2-vinylpyrindine) (PS-*b*-P2VP) and polyferrocenylsilane-*b*-poly(2-vinylpyrindine) (PFS-*b*-P2VP) BCPs by living anionic polymerization. The pronounced microphase separation capability for these amphiphilic metal-containing BCPs is investigated as a functional template for the preparation and *in situ* functionalization of silica mesoporous films. End-functionalized BCPs featuring triethoxysilane groups are studied with respect to their feasibility for a co-condensation approach via EISA. Moreover, the prepared polymer-silica hybrid films are investigated with respect to the ionic permselectivity in dependence on pH value variations that are based on the stimulus-responsiveness of the P2VP block segment.

EXPERIMENTAL SECTION.

Reagents. All of the solvents and reagents were purchased from Alfa Aesar (Haverhill, MA), Sigma-Aldrich (St. Louis, MA), Fisher Scientific (Hampton, NH), and ABCR (Karlsruhe, Germany) and used as received unless otherwise stated. Tetrahydrofuran (THF) was distilled from sodium/benzophenone under reduced pressure prior to the addition of 1,1'-diphenylethylene (DPE) and *n*-butyllithium (*n*-BuLi) followed by a second distillation. Styrene and 2-vinylpyridine

were dried by stirring over calcium hydride or trioctylaluminium and distilled prior to use. The 1,1'-dimethylsilaferrocenophane (FS) was synthesized and purified as described elsewhere.[47] Lithium chloride was dissolved in a small amount of purified THF and placed into an ampule. After removing the THF in vacuum, the ampule was carefully heated in a high vacuum, refilled with nitrogen, and stored in a glovebox. The 1,1'-diphenylethylene (DPE) was distilled after titration with *n*-BuLi from solution. The 1,1'-dimethylsilacyclobutane (DMSB) and silicon tetrachloride were stirred over CaH_2 and distilled. All syntheses were carried out under a protective atmosphere of nitrogen using Schlenk techniques or a glovebox equipped with a Coldwell apparatus.

NMR. NMR spectra were recorded with a Bruker DRX 500 NMR (Billerica, MA) or with a Bruker DRX 300 spectrometer working at 500 or 300 MHz (^{1}H NMR), respectively.

Standard SEC. Size exclusion chromatography (SEC) was performed with a system composed of a 1260 IsoPump – G1310B - (Agilent Technologies, Santa Clara, CA, USA), a 1260 VW-detector – G1314F – at 254 nm (Agilent Technologies) and a 1260 RI-detector – G1362A – at 30 °C (Agilent Technologies), and THF as the mobile phase (flow rate 1 mL min^{-1}) on a SDV column set from PSS (Polymer Standard Service (PSS), Mainz, Germany) (SDV 10^3, SDV 10^5, and SDV 10^6). The calibration was carried out using PS standards (from Polymer Standard Service, Mainz).

IR spectroscopy. IR spectroscopy was performed on a Spectrum One instrument (PerkinElmer) (Waltham, MS) in attenuated total reflection (ATR) mode. The IR spectra were recorded from 4000 to 650 cm^{-1}. The measured spectra were automatically background-corrected and normalized to the Si-O-Si band at ~1070 cm^{-1}.

Differential scanning calorimetry (DSC). DSC was used to determine the thermal properties of the synthesized polymers with a Mettler Toledo DSC1 (Columbus, OH) over a temperature range from 100-180 °C with a heating rate of 10 K min^{-1} under nitrogen atmosphere.

Thermogravimetric analysis (TGA). TGA was applied by using a Mettler Toledo TGA-2 (Columbus, OH) with a heating rate of 10 K/min over a range from 30-600 °C in a nitrogen or air atmosphere.

Cyclic voltammetry (CV). CV measurements are performed with a 1 mM solution of the respective probe molecule in an aqueous 100 mM KCl supporting electrolyte solution. The pH was adjusted with NaOH or HCl. An Ag/AgCl electrode was used as the reference electrode, and various scan rates between 25 mV/s and 1000 mV/s were measured. The measured electrode area was 0.21 cm^2.

Dynamic light scattering (DLS). DLS results were obtained using a Zetasizer Nano ZS90 (Malvern, UK) using a cumulant fit (for all DLS data of the main manuscript), while for determination of the CMC (Supporting Information) the DLS experiments were carried out with an apparatus based on a He−Ne laser ($\lambda = 632.8$ nm) as the light source. Polarization of the primary beam was defined by a Glan-Thomson prism. The scattered beam polarization was analysed in a vertical−vertical geometry. The scattered intensity was detected with an optical fibre coupled to two avalanche photodiodes. The intensity autocorrelation functions, calculated with ALV 5000 software for both photodiodes, were measured in angular steps of 10°. All measurements were performed by using cylindrical cuvettes (Hellma) for the samples in a temperature-controlled index matching bath. The intensity autocorrelation functions can be described by a stretched exponential decay (KWW-function):

$g^2 - 1 = (A*\exp(-(t/\tau)^{\beta}))^2 + C$

Where A describes the amplitude of the process, τ is the correlation time and β is the stretching parameter, which corresponds to the polydispersity of the particles. For example, if β is equal to 1, the particles are ideally monodispersed. The averaged correlation time is $<\tau> = \tau/\beta*\Gamma(1/\beta)$, while Γ is the gamma function, $<\tau>$ is related to the translational diffusion coefficient D by $D = 1/(<\tau>q^2)$, and the scattering vector q can be calculated by $q = 4\pi n\sin(\theta)/\lambda$. In our case, n is the refractive index of ethanol and 2θ is the scattering angle.

Transmission electron microscopy (TEM). TEM experiments were carried out using a Zeiss EM 10 electron microscope (Oberkochen, Germany) with an operating voltage of 60 kV. For the investigation of single particles, diluted dispersions were drop-cast on carbon-coated copper grids followed by drying at room temperature.

Scattering electron microscopy (SEM). SEM measurements were conducted on a Philips XL30 FEG (Philips, Amsterdam, The Netherlands) with accelerating voltages between 5 and 30 kV. The samples were coated with approximately 4 nm Pt/Pd (ratio 80/20) using a Cressington 208HR sputter coater.

Anionic Block Copolymerization of Styrene and 2-Vinylpyridine and End-functionalization (PS_{134}-*b*-$P2VP_{282}$-$Si(OEt)_3$). In an ampule equipped with a stirring bar, 500 mg (4.8 mmol) of styrene was dissolved in 25 mL of dry THF (with dissolved lithium chloride and *sec*-butyllithium) and the solution was cooled to -78 °C. The polymerization was initiated by a quick addition of 38 µL of *sec*-Buli (0.05 mmol, 1.3 M solution in hexane) using a Hamilton syringe. The solution was stirred for 1 h to ensure complete conversion. After taking an aliquot for SEC measurement, 500 mg (4.8 mmol) of precooled (-20 °C) 2-vinylpyridine was quickly added with a syringe and

the reaction was stirred for 1.5 h at -78 °C. To the living chain, 28.7 µL (0.25 mmol) silicon tetrachloride was added and stirred for 0.5 h, and then 373 µL sodium ethoxide (21-% solution, 1 mmol) was added for the conversion to the triethoxy silane end group. We note that for BCP PS_{134}-*b*-$P2VP_{282}$-$Si(OEt)_3$, the DPE functionalization step was skipped, as there is – compared to the metallopolymer-based BCPs – no necessity.

The generated polymer was precipitated into 10-fold excess of water and subsequently collected by filtration, washed with water and dried under vacuum. SEC (vs P S) results for the PS-precursor were M_n = 14000 g/mol, M_w = 26700 g/mol, and $Đ$ = 1.91; the results for the PS-*b*-P2VP-$Si(OEt)_3$ were M_n = 20500 g/mol, M_w = 28500 g/mol, and $Đ$ = 1.39.

Anionic Block Copolymerization of 1,1'-Dimethylsilaferrocenophane and 2-Vinylpyridine with end group functionalization (PFS_{13}-*b*-$P2VP_{167}$-$(SiOEt)_3$). In an ampule equipped with a stirring bar, 200 mg (0.82 mmol) of 1,1'-dimethylsilaferrocenophane was dissolved in 5 mL of dry THF followed by a quick addition of 12.5 µL of *n*-BuLi (0.02 mmol, 1.6 M solution in hexane) in a Hamilton syringe. After 3 h of reaction time at room temperature, an aliquot for SEC measurements was taken. The quantities of 14.1 µL (0.08 mmol) 1,1'-diphenylethylene and 5.16 µL (0.04 mmol) 1,1'-dimethylsilacyclobutane were transferred to the solution. The solution turned to a deep red colour. The so-called concept of the carbanion-pump was applied to guarantee the efficient block copolymerization of reactivated PFS chains with the DPE moiety followed by the subsequent polymerization of 2VP in the next step.[47] This strategy enables the preparation of well-defined PFS-P2VP-based BCPs.

This macroinitiator was given to a precooled solution of 200 mg (2 mmol) 2-vinylpyridine in THF at -78 °C. After 2 h, 7.1 µL (0.04 mmol) 1,1'-diphenylethylene was added and heated to room

temperature. After 0.5 h, the solution was cooled to -78 °C again, and 11.5 µL (0.1 mmol) silicon tetrachloride was added to the living chain and stirred for 0.5 h. Then, 149.3 µL sodium ethoxide (21-% solution, 0.4 mmol) was added for the conversion to the triethoxy silane end group.

The polymer was precipitated into a 10-fold excess of water. The polymer was collected by filtration, washed with water and dried under vacuum. The SEC (vs PS) results for the PFS-precursor were M_n = 3200 g/mol, M_w = 4400 g/mol, and $Đ$ = 1.37; the results for the PFS-*b*-P2VP-$Si(OEt)_3$ were M_n = 7000 g/mol, M_w = 15600 g/mol, and $Đ$ = 2.23. The ^{1}H NMR results (300 MHz, 300 K, $CDCl_3$, chem. shift (δ) in ppm) were 0.56 (s, Si(CH3)2), 1.78-2.34 (m, CH2 and CH, P2VP), 4.01 (m, Cp), 4.21 (m, Cp), 6.35-7.2 (m, arom. protons, P2VP), and 8.09-8.41 (m, NCHC).

Film Preparation. Mesoporous silica films were synthesized via a sol-gel method based on the oxide precursor tetraethyl orthosilicate (TEOS) in the presence of the template PS-*b*-P2VP-$Si(OEt)_3$ and PFS-*b*-P2VP-$Si(OEt)_3$. The precursor solution was stirred for 24 h and used to produce films using evaporation-induced self-assembly (EISA)[22] on indium tin oxide (ITO)-coated glass, glass or silicon wafer substrates at 40-50% relative humidity and 298 K with a withdrawal speed of 2 mm/s. The precursor solution was prepared using the following molar ratios: 1 TEOS: 0.0005 polymer: 40 ethanol: 10 water: 0,0021 HCl. For the films prepared with PFS-*b*-P2VP-$Si(OEt)_3$, no hydrochloric acid was used.

The furnace program was used until 500 °C was reached to calcite the porous silica completely so that the templates burned out. Freshly deposited films were stored at 50% relative humidity in a chamber for 1 h. Then, a stabilizing thermal treatment was carried out in two successive 1 h steps at 60 °C and 130 °C. Consecutively, the temperature was increased to 500 °C with a gradient of 1 °C min^{-1}. The films were finally stabilized at 500 °C for 2 h.

The furnace program was used until 200 °C was reached when the template should be in the pores after the film was prepared. Freshly deposited films were stored at 50% relative humidity in a chamber for a minimum of 1 h. Then, a stabilizing thermal treatment was carried out in two successive 1 h steps at 60 °C and 130 °C. The temperature was ramped up from 130 to 200 °C at 1 °C min^{-1}. Finally, films were stabilized at 200 °C for 2 h.

RESULTS AND DISCUSSION

To achieve *in situ* functionalization of mesoporous separation layers, PFS-*b*-P2VP and PS-*b*-P2VP were used as functional templates during mesoporous film preparation with EISA in ethanol. While P2VP as a hydrophilic block offers pH responsiveness, PFS represents the hydrophobic block and implements redox responsivity. Moreover, the metal-containing segment can be selectively removed upon treatment with hydrochloric acid, allowing for free pore volume generation. By this strategy, transport within the P2VP-functionalized mesopores can be facilitated (Scheme 1).[48, 49] Volume fractions of 30% PFS and 70% P2VP were chosen to gain access to spherical micelles in ethanol.[50] To covalently attach the P2VP block into the mesopore silica wall during film preparation, PFS-*b*-P2VP-$Si(OEt)_3$ was prepared using end group capping with silicon tetrachloride and conversion with sodium ethoxide (Scheme 1).

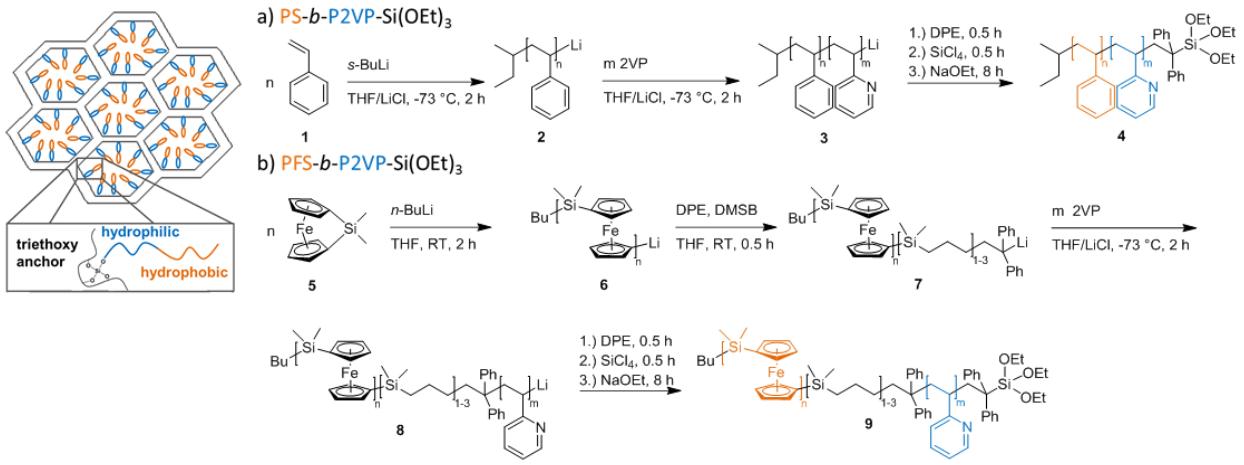

Scheme 1. Concept of BCP synthesis as a template for *in situ* mesopore functionalization. a) Synthetic pathway leading to PS-*b*-P2VP-Si(OEt)$_3$ (4) by sequential anionic polymerization of styrene and 2-vinylpyridine followed by end-capping and work-up in the presence tetraethoxysilane. b) Synthetic strategy leading to PFS-*b*-P2VP-Si(OEt)$_3$ (9) by sequential anionic polymerization of 1,1'-dimethylsilaferrocenophane and 2-vinylpyridine followed by end-capping and work-up with tetraethoxysilane.

Polymer synthesis and characterization. Amphiphilic block copolymers PS-*b*-P2VP-Si(OEt)$_3$ and PFS-*b*-P2VP-Si(OEt)$_3$ were synthesized by sequential anionic polymerization, as shown in Scheme 1. To generate the desired triethoxysilane end-group, the active polymer chains were treated with tetrachlorosilane followed by conversion with sodium ethoxide. The respective BCPs PS-*b*-P2VP-Si(OEt)$_3$ that had molecular weights up to 132 000 g/mol and P2VP contents between 33 - 68 mol% were prepared and characterized by ^{1}H NMR spectroscopy and SEC (Table S1 in SI). To further prove the presence of the silane end group model, P2VPs were identically prepared and investigated by using MALDI-ToF MS, NMR and SEC (Scheme S1, Figures S1 and S2 in SI). A dispersity index value, *Đ,* of 1.08-1.39 was determined, suggesting that a controlled polymerization procedure occurred. The metallopolymer-containing BCPs with P2VP as the second block segment (PFS-*b*-P2VP) and the corresponding end-functionalized diblock copolymer PFS-*b*-P2VP-Si(OEt)$_3$ were also prepared by sequential anionic polymerization (cf. the experimental section). All data on the investigated polymers and BCPs are compiled in Table 1. Molar masses of up to 35 500 g/mol featuring a P2VP content of 80-90 mol% and a dispersity

index value of $Đ = 1.1$ were obtained. A rather high P2VP content was chosen to achieve a micellar shape, which is capable of mesoporous film formation using evaporation-induced self-assembly (EISA), as discussed below.[22] The presence of the silane end group is demonstrated by differences in the DSC and ^{1}H NMR spectroscopy results, as shown in the Supporting Information (Figures S1, S3, S4 and S5). Additionally, covalent binding of PFS-*b*-P2VP-Si(OEt)$_3$ to planar, dense silica films could be successfully demonstrated, whereas this was not observed during the monitoring of the PFS-*b*-P2VP static contact angle (Table S2 in SI). This indicates successful end-capping of the PFS-*b*-P2VP with the silane anchoring sites. Furthermore, a variation in the pH resulted in a Young's contact angle change of approximately 10°, demonstrating pH-induced switching between neutral and positively charged polymers due to protonation of the P2VP block.

Table 1. Overview of all homopolymers, BCPs and functionalized BCPs synthesized in the present study. Additional BCPs can be found in the supporting information (Table S1).

Polymer	$M_{n,exp}$ (g/mol)[a]	$M_{w,exp}$ (g/mol)[a]	$Đ$[a]	x_{P2VP} (%)	w_{P2VP} (%)	$Φ_{P2VP}$ (%)
PS$_{125}$	13 000	13 800	1.06			
PS$_{125}$-*b*-P2VP$_{125}$-Si(OEt)$_3$	28 200	30 400	1.08	50.2	50.4	48.2
PS$_{834}$	86 900	93 500	1.08			
PS$_{834}$-*b*-P2VP$_{827}$-Si(OEt)$_3$	132 100	159 700	1.21	50.0	50.2	47.0
PFS$_{77}$	18 600	19 200	1.04			
PFS$_{77}$-b-P2VP$_{972}$	34 600	38 200	1.1	84.6	70.4	72.3
PFS$_{77}$-*b*-P2VP$_{989}$-Si(OEt)$_3$	35 500	39 100	1.1	84.8	70.7	73.6
PFS$_{12}$	3 000	3 400	1.13			
PFS$_{12}$-*b*-P2VP$_{229}$-Si(OEt)$_3$	20 600	21 700	1.06	88.0	77.6	79.2

[a] Molecular weight and $Đ$ determined by SEC in g/mol (PS standards, THF) for the PS precursor and the BCPs. $Đ$ values correspond to the BCP. x, w and Φ are molar, weight and volume content of the BCP in %, respectively. ^{1}H NMR spectroscopy (300 Hz, $CDCl_3$) data were used to calculate the composition of the respective BCPs.

Polymer micelle characterization. To investigate BCP micelle formation, the polymers were dissolved in different solvents, as described in the experimental section. The resulting PS$_{134}$-*b*-P2VP$_{282}$-Si(OEt)$_3$ and PFS$_{13}$-*b*-P2VP$_{167}$-Si(OEt)$_3$ micelles were characterized using DLS and TEM (Figure 1). For this purpose, PS$_{134}$-*b*-P2VP$_{282}$-Si(OEt)$_3$ was dissolved in THF or ethanol at

varying concentrations to analyse the micellar shape using dynamic light scattering (Figure 1a) and TEM (Figure 1b). The critical micellar concentration (cmc), which is an important parameter with respect to mesoporous film formation by EISA, was observed to be below the resolution of the DLS apparatus, *i.e.*, it was lower than 0.2 mg/mL. The micelle diameter is dependent on the solvent due to the different selectivity and dissolving power of solvents, resulting in different hydrodynamic volumina of the micelles. Based on the relevant EISA film formation conditions, ethanol or ethanol/THF were investigated as solvents. THF, another well-established EISA solvent, is not suitable for PFS-*b*-P2VP BCPs, as it is a good solvent for both blocks, P2VP and PFS. Whereas ethanol micelle diameters of 38.5 nm (±1 nm) were observed using TEM (Figure 1c-e), the addition of 8 vol% THF led to a micelle diameter increase up to 52.5 nm (±0.5 nm) (Figure 1a). This can be explained by the selective interaction of ethanol with the P2VP block resulting in corona swelling, whereas THF is a good solvent for both blocks.

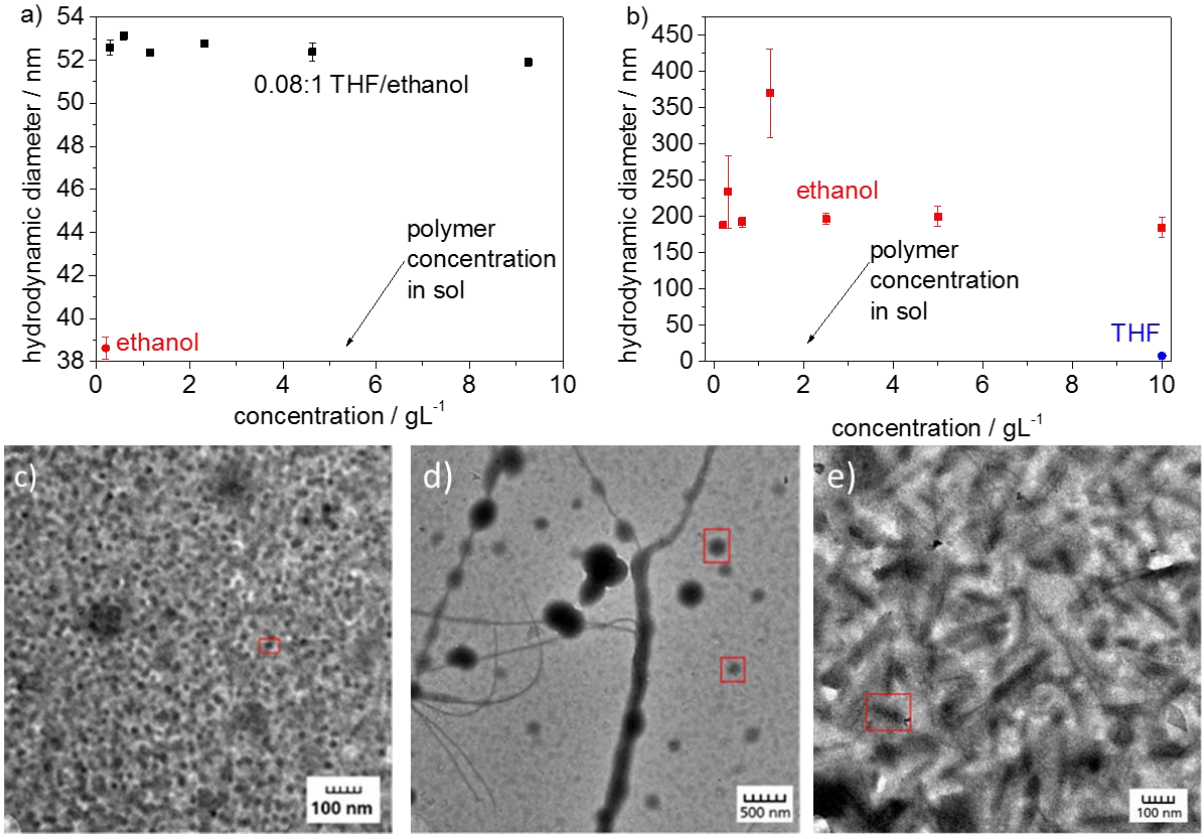

Figure 1. Concentration-dependent micelle diameter obtained by DLS for the **a)** PS_{134}-*b*-$P2VP_{282}$-$Si(OEt)_3$ and **b)** PFS_{13}-*b*-$P2VP_{167}$-$Si(OEt)_3$ polymers. **c)** TEM image of the PS_{134}-*b*-$P2VP_{282}$-$Si(OEt)_3$ micelles in ethanol. The PS_{134}-*b*-$P2VP_{282}$-$Si(OEt)_3$ micellar size seems to be independent of the concentration in ethanol, showing a micellar diameter of ~ 38.5 nm. **d)** Representative TEM images of the $PFS_{15\%}$-*b*-$P2VP_{85\%}^{7000g/mol}$ micelles before ultrasonic treatment in ethanol and **e)** representative TEM image of $PFS_{15\%}$-*b*-$P2VP_{85\%}^{7000g/mol}$ micelles after ultrasonic treatment in ethanol showing the cutting of micellar fibres into shorter elongated micelles.

Dissolving the PFS_{13}-*b*-$P2VP_{167}$-$Si(OEt)_3$ BCP in THF or ethanol with varying concentrations resulted in relatively large diameters (Figure 1b and Figure S6) of 188 ± 15 nm in ethanol, probably due to aggregate formation of spherical or formanisotropic micelles, and very small diameters in THF. The small micelle diameters in THF can be explained by THF being a good solvent for both blocks, giving a hydrodynamic radius of 8.0 ± 0.3 nm for PFS_{13}-*b*-$P2VP_{167}$-$Si(OEt)_3$ and 8.5 ± 0.3 nm for PFS_{12}-*b*-$P2VP_{229}$-$Si(OEt)_3$. In addition, the cmc for the PFS_{13}-*b*-$P2VP_{167}$-$Si(OEt)_3$ BCP seems to be very low and below the lowest measured concentration of 0.0026 wt%. Furthermore, concentration independent micelle diameters are observed by DLS in ethanol/THF~~, indicating the~~

~~presence of spherical micelles~~. The absence of cylindrical micelles, which would be expected for this type of block copolymer[50,] can be explained by the sample preparation process containing a filtration (syringe filter) step. Without filtration, cylindrical micelles are clearly present as well (Figure 1e). These cylindrical micelles can be converted into rod-like micelles with diameters of 20-30 nm and a length of approximately 100 nm using an ultrasonic treatment, which is in agreement with reports by Manners and co-workers. For cylindrical micelle formation, the solvent composition and the volume fraction of the respective BCP segments PFS and P2VP are crucial parameters, as shown earlier.[50, 51]

Porous film formation. The obtained BCP micelles were used for the *in situ* functionalization of nanoscale pores to generate functional pores with controlled transport characteristics within one fabrication step. This process requires well-defined polymers to obtain a homogeneous mesopore size distribution. BCPs with the silane end group can be covalently attached to the silica mesopore wall. Therefore, the end group of the responsive block was chosen to show a comparable reactivity to the silica precursor forming the mesopore wall. It is important to adjust the film preparation temperatures to the BCP stability, which was evaluated by thermal gravimetric analysis (TGA) (Figure S7, SI). ~~Porous films were obtained using the above described polymers as templates in an ethanolic solution containing TEOS:polymer:EtOH:H_2O:HCl = 1:0.0075:40:10. The polymer was first dissolved in approximately 0.1 mL of THF before being added to the solution. For the PFS-containing block copolymer formulations, no acid (HCl) was used because of the acid-induced degradation of PFS. Dip-coating the induced EISA of these solutions was performed under environmentally controlled conditions (50% RH and 25 °C)~~. Based on the thermal gravimetric analysis results showing a stable block copolymer up to 300 °C and full degradation at 500 °C (see Figure S7), a final calcination temperature of 200 °C was chosen. Reference films with a fully

removed template were treated up to a final calcination temperature of 500 °C. The resulting film morphology and structure were analysed by scanning electron microscopy (SEM), transmission electron microscopy (TEM) and ellipsometry (Figure 2, S8 and S9). After removal of the BCP template at 500 °C (Figure 2a, b, d, e, S10), a mesoporous structure was clearly visible for both types of block copolymer templates. The accessibility and mesoscopic size of this porous structure was indirectly confirmed by cyclic voltammetry (Figure 3b and S11, S12); electrostatic exclusion of negatively charged probe molecules were shown at a basic pH. This indicates pore sizes in the range of the Debye screening length. Interestingly, the dimensions of the observed porous structure did not directly correlate to the observed micellar size (Figure 1, 2). This supports observations in the literature of the silica precursor (TEOS) interaction and mixing with the hydrophilic P2VP block, resulting in the much smaller observed mesopore size (Figure 2) than the detected micellar size (Figure 1).[52, 53] This interpretation is supported by mesoporous films generated resulting from PFS-*b*-P2VP without silane end groups. (Figure 2 f). PFS-*b*-P2VP without an end group revealed similar mesopore structures with a comparable pore accessibility to that of the PFS-*b*-P2VP-$Si(OEt)_3$, as detected by cyclic voltammetry (Figure S13, SI). Figure 2c shows a mesoporous film templated by PFS_{12}-*b*-$P2VP_{229}$-$Si(OEt)_3$ treated up to 200 °C that still contained the BCP template within the mesopores that resembled a closed film surface in the TEM image (Figure 2f). This also corresponds to the blocked mesopore accessibility that was observed by cyclic voltammetry (Figure S14).

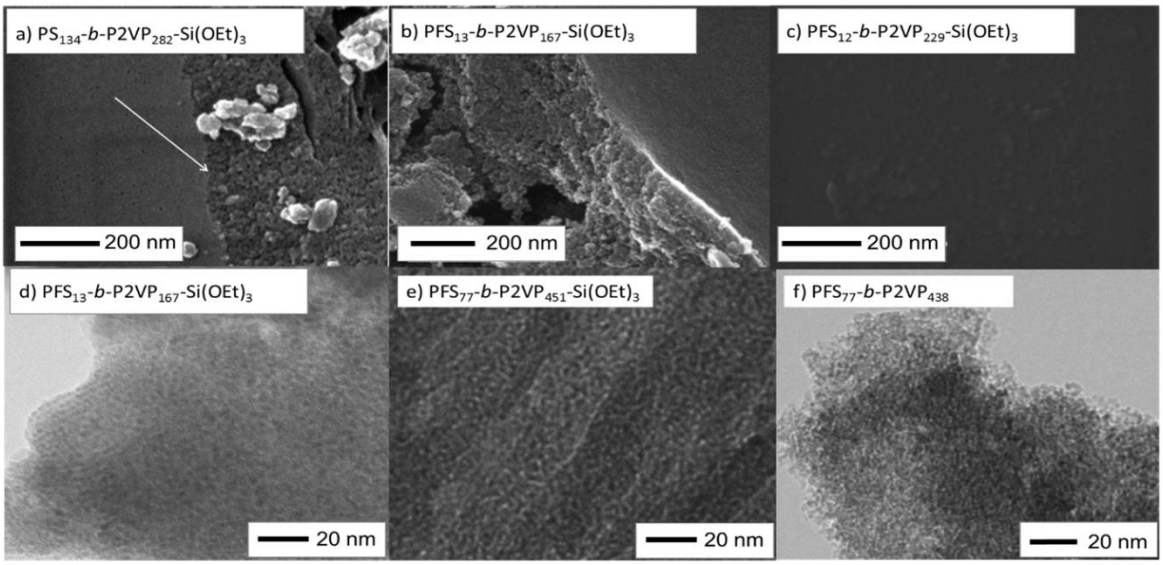

Figure 2. a) SEM image of a PS_{134}-*b*-$P2VP_{282}$-$Si(OEt)_3$-templated silica film after burning the template at 500 °C**. b)** SEM image of the silica film prepared with PFS_{13}-*b*-$P2VP_{167}$-$Si(OEt)_3$ after burning the template at 500 °C. **c)** SEM image of a PFS_{12}-*b*-$P2VP_{229}$-$Si(OEt)_3$-templated silica film with a template that was treated to 200 °C**. d)** TEM image of a PFS_{13}-*b*-$P2VP_{167}$-$Si(OEt)_3$-templated silica film after burning the template at 500 °C**. e)** TEM image of a PFS_{77}-*b*-$P2VP_{451}$-$Si(OEt)_3$-templated silica film after burning the template at 500 °C, showing structural order at the nanoscale. **f)** TEM image of a PFS_{77}-*b*-$P2VP_{438}$-templated silica film after burning the template at 500 °C.

Transport into *in situ* functionalized mesopores. The accessibility of the *in situ* functionalized silica films was measured using cyclic voltammetry that monitored the presence of $[Ru(NH_3)_6]^{2+/3+}$ and $[Fe(CN)_6]^{3-/4-}$ redox probe molecules (0.1 mM) at an electrode located below the functionalized silica film at pH ≤ 3 or pH ≥ 9. At pH ≤ 3, the silica was almost neutrally charged (pK_a ~ 2-4)[54-56], which should allow access to both probe molecules, resulting in a detectable peak current (Ip). At pH ≥ 9, the silica was negatively charged, which induced the electrostatic exclusion of identically charged $[Fe(CN)_6]^{3-/4-}$ in the case of pore sizes in the range of the Debye screening length; thus, overlapping electric double layers formed. Under these conditions, the countercharged $[Ru(NH_3)_6]^{2+/3+}$ should be preconcentrated into the mesopores due to electrostatic attraction. In the case of block copolymer-functionalized pores, the film accessibility is additionally dependent on the available free pore volume, wettability, and polymer charge. The pK_s value of the P2VP was expected to be 4.5.[57] Based on this, a positively charged pore in acidic

solution with a pH value below 4.5, an electrostatic exclusion of $[Ru(NH_3)_6]^{2+/3+}$ and a pre-concentration of $[Fe(CN)_6]^{3-/4-}$ was expected. At basic pH, the pores were expected to be neutral (P2VP) or negatively charged if accessible silanol groups at the pore wall surface still existed. In the case of a neutral and accessible pore identical behaviour and comparable peak current densities for both probe molecules would be expected, whereas a negatively charged pore was expected to electrostatically exclude $[Fe(CN)_6]^{3-/4-}$ if the pore size was small enough to pre-concentrate the countercharged $[Ru(NH_3)_6]^{2+/3+}$.

PS_{134}-*b*-$P2VP_{282}$-Si(OEt) – based films. Figure 3a shows the recorded cyclic voltammograms of the PS_{134}-*b*-$P2VP_{282}$-$Si(OEt)_3$ templated silica film (film thickness 50 nm) before template removal. Neither $[Ru(NH_3)_6]^{2+/3+}$ (red) nor $[Fe(CN)_6]^{3-/4-}$ (blue) are able to reach the bottom electrode independent of the applied solution pH; this is indicated by resulting in a detectable peak current density (j_p) in a defect-free porous film is obtained. This is supported by the observed silica pH-dependent ionic permselectivity and the electrostatic exclusion of the $[Fe(CN)_6]^{3-/4-}$ at pH 9 from the nanoscale pores after the calcination, which burned out the PS_{134}-*b*-$P2VP_{282}$-$Si(OEt)_3$ polymer template (Figure 3b). Full electrostatic exclusion with accessible pores at an acidic pH can only be expected for nanoporous films without defects larger than the Debye screening length and pore sizes in the range of the Debye screening length. Only the pre-concentration of $[Ru(NH_3)_6]^{2+/3+}$ (red) at pH 9 was less pronounced than that of the other mesoporous silica materials,[28, 29, 54, 58, 59] which indicates a decreased silanol group density on the surface. This resulted from the high calcination temperature of 500 °C that was applied to remove the PS_{134}-*b*-$P2VP_{282}$-$Si(OEt)_3$ polymer template. Usually, calcination temperatures of up to 350 °C are used.[29, 54, 60, 61]

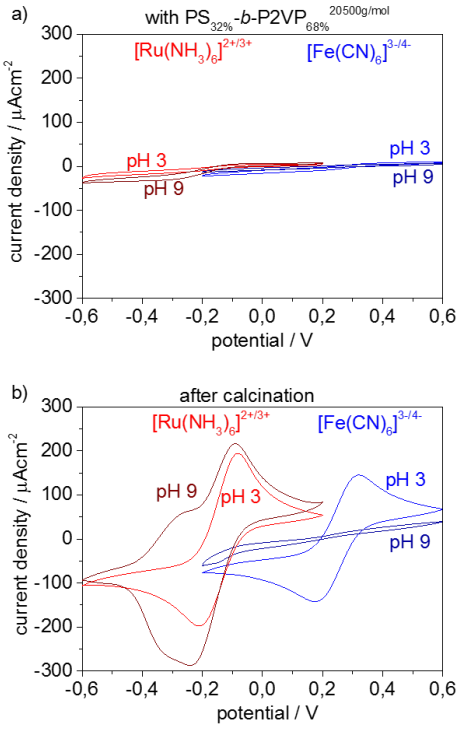

Figure 3. a) Cyclic voltammetry studies (with a scan rate of 100 mV/s) of the molecular transport through PS_{134}-*b*-$P2VP_{282}$-$Si(OEt)_3$-templated silica thin films using $[Ru(NH_3)_6]^{2+/3+}$ (red) and $[Fe(CN)_6]^{3-/4-}$ (blue) as ionic redox probes that indicate defect-free non-accessible films. **b)** Cyclic voltammograms recorded in analogy to (a) after PS_{134}-*b*-$P2VP_{282}$-$Si(OEt)_3$ template calcination at 500 °C that show pH-dependent nanopore accessibility. Electrolyte: 1 mM redox probe and 0.1 M KCl (pH 3 and 9).

PFS_{13}-*b*-$P2VP_{167}$-$Si(OEt)_3$- and PFS_{12}-*b*-$P2VP_{229}$-$Si(OEt)_3$-based films. The same behavior of inaccessible films before template removal and silica nanopore like electrostatically controlled film accessibility is observed for PFS_{13}-*b*-$P2VP_{167}$-$Si(OEt)_3$ -templated silica films (pH 9, Figure S14). In accordance with the Randles-Sevcik equation, a linear relation of peak current density versus square root of the scan rate was observed after burning out the PFS_{13}-*b*-$P2VP_{167}$-$Si(OEt)_3$ and PFS_{12}-*b*-$P2VP_{229}$-$Si(OEt)_3$ templates for the measured scan rates between 25 mV/s and 1000 mV/s (Figure S11), indicating a diffusion-limited transport process.

To prove the selective dissolution of the PFS block at an acidic pH in the presence of HCl, cyclic voltammetry was performed in the absence of probe molecules (100 mM KCl electrolyte). The

degradation of the PFS in the mesoporous silica without the use of electrochemistry is shown in Figure S15 (SI) by contact angle measurements.

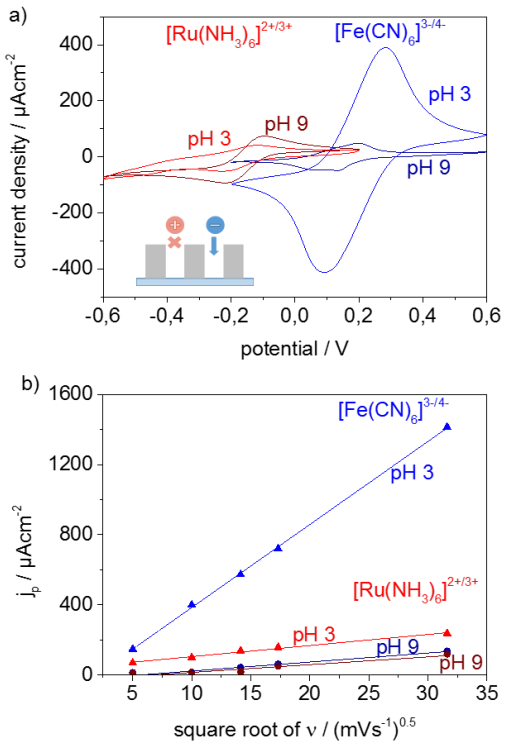

Figure 4. a) Cyclic voltammetry studies (with a scan rate 100 mV/s) of the molecular transport through the porous silica thin films after PFS cleavage of the PFS_{12}-*b*-$P2VP_{229}$-$Si(OEt)_3$ template with HCl using $[Ru(NH_3)_6]^{2+/3+}$ (red) as a cationic redox probe and $[Fe(CN)_6]^{3-/4-}$ (blue) as an anionic redox probe. Electrolyte: 1 mM redox probe and 0.1 M KCl (pH 3 and 9). **b)** Peak current density as a function of the square root of the scan rate according to the Randles-Sevcik equation for pH values 3 (triangle) and 9 (circles) for both probe molecule complexes $[Ru(NH_3)_6]^{2+/3+}$ (red) and $[Fe(CN)_6]^{3-/4-}$ (blue), showing a linear dependence for the measured scan rates between 0.025 and 1 V/s.

At basic and neutral pH values, the absence of a peak current indicates the presence of filled pores with intact BCPs. The addition of HCl immediately destroyed the PFS blocks, which resulted in a peak current at -0.6 V, most likely corresponding to PFS fragments (Figure 4, Figure S16). This is proof of the presence of PFS inside the silica film, its accessibility to HCl and the removal of the PFS blocks (see Figures S14 and S17, SI). The observed results agree with PFS degradation reported by Manners and co-workers. They reported that Fe-Cp bond cleavage occurred when PFS

was oxidized by a minimum of 10% in the presence of nucleophilic species.[62-64] After complete PFS block extraction with HCl, the cyclic voltammogram of the remaining film showed a pH-dependent accessibility of the $[Ru(NH_3)_6]^{2+/3+}$ and $[Fe(CN)_6]^{3-/4-}$ probe molecules corresponding to positively charged nanopores at pH ≤ 3 and pH ≥ 9, which resulted from the PVP blocks left in the silica film (Figure 4a). Therefore, the positively charged probe molecule $[Ru(NH_3)_6]^{2+/3+}$ was electrostatically excluded at pH ≤ 3 as well as at pH 9, but a small accessibility (j_p) was still observed, indicating a second P2VP-free path towards the bottom electrode. Additionally, the redox peak potential shifts which seems to indicate electrostatic attraction as generally observed for mesoporous silica films.[54, 65] The observed j_p at pH ≤ 3 was slightly smaller than that observed for $[Ru(NH_3)_6]^{2+/3+}$ and $[Fe(CN)_6]^{3-/4-}$ at pH ≥ 9, where neutral P2VP was expected. The absence of the pre-concentration of $[Ru(NH_3)_6]^{2+/3+}$ at pH ≥ 9 indicates the absence or inaccessibility of negatively charged SiO groups at the pore wall and a P2VP-controlled transport process. This is supported by the observed significant pre-concentration of $[Fe(CN)_6]^{3-/4-}$ at pH ≤ 3, which has a j_p that is factor of 22 higher than that at pH ≥ 9. In addition, this j_p shows a clear pre-concentration of $[Fe(CN)_6]^{3-/4-}$ at pH ≤ 3 compared to that for the films after the entire template was burned out. Therefore, only 12 mol% of the polymer template comprised PFS; thus, 85 mol% of the pores were filled with P2VP, which was strongly confined. These results prove the successful *in situ* functionalization and the feasibility of this concept for transport control through nanopores.

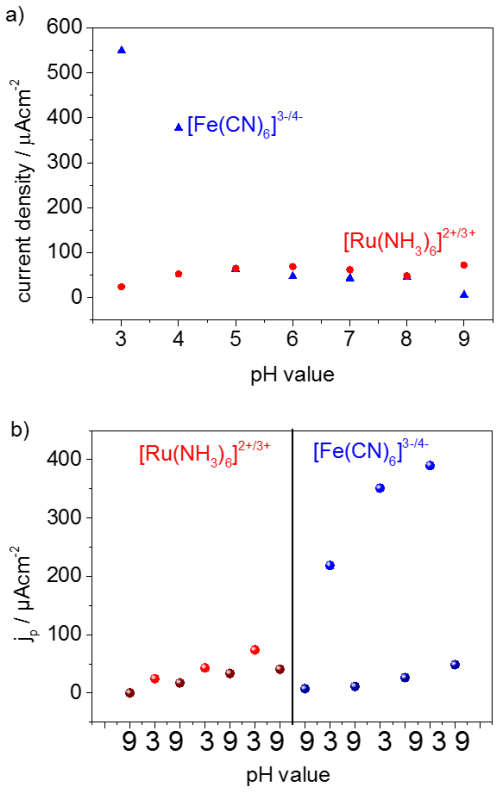

Figure 5. a) Cyclic voltammetry studies (with a scan rate 100 mV/s) of the molecular transport through the porous silica thin films after PFS cleavage of the PFS_{13}-*b*-$P2VP_{167}$-$Si(OEt)_3$ template with HCl using $[Ru(NH_3)_6]^{2+/3+}$ (red traces) as a cationic redox probe and $[Fe(CN)_6]^{3-/4-}$ (blue traces) as an anionic redox probe. Electrolyte: 1 mM redox probe and 0.1 M KCl (pH 3 to 9). **b)** The determined peak current plotted against pH values of 3 (light colour) and 9 (dark colour) for both probe molecule complexes $[Ru(NH_3)_6]^{2+/3+}$ and $[Fe(CN)_6]^{3-/4-}$ to show the PFS cleavage.

Furthermore, the titration of the pore accessibility revealed a clear pH tuneable transport for $[Fe(CN)_6]^{3-/4-}$ between pH 3 and 6, which corresponds to the pK_a value of the P2VP and thus, a change in the charge density (Figure 5a). This indicates a broad pH transition, which corresponds to theoretical studies of polyelectrolytes in the spatial confinement of nanopores.[66] A repetition of the pH-gating over three cycles (Figure 5b) showed further activation of the pores based on a slightly increasing j_p with repeated switching between pH 3 and pH 9, which might have resulted from the high pore filling with P2VP based on the block copolymer content of 85-88 mol% P2VP. Nevertheless, the general trend of a high $[Fe(CN)_6]^{3-/4-}$ preconcentration at an acidic pH with a

positively charged P2VP and a substantially decreased pore accessibility in the presence of neutral P2VP or for positively charged $[Ru(NH_3)_6]^{2+/3+}$ at a basic and an acidic pH remains

CONCLUSION. In summary, a series of functional block copolymers of styrene and 2--vinylpyridine as well as 1,1'-dimethylsilaferrocenophane and 2-vinylpyridine with a triethoxysilane end group each were synthesized. Micelle formation resulted in BCP spheres or cylinders in ethanol/THF depending on the BCP composition. The subsequent application as a functional template rendered *in situ* functionalized mesoporous silica films with interesting transport properties. Functional template-filled pores were hydrophobic and inaccessible for small ions. The redox-mediated degradation of the PFS block segment resulted in P2PVP-functionalized mesopores with pH-responsive transport properties. The calcination at 500 °C formed empty mesopores with mesopore transport characteristics that were controlled by the silanol groups.

ASSOCIATED CONTENT

Supporting Information.

The following files are available free of charge: Details regarding characterization of the blockcopolymers and investigation of the end group functionalization. Further measurements of ionic perm selectivity trough the hybrid mesoporous silica films as well as contact angle measurements are provided. (PDF)

AUTHOR INFORMATION

Corresponding Author

*E-Mail: andrieu-brunsen@smartmem.tu-darmstadt.de (A. A.-B.) markus.gallei@uni-saarland.de (M. G.)

Author Contributions

The manuscript was written through contributions of all authors. All authors have given approval to the final version of the manuscript.

Notes

The authors declare no competing financial interest.

Funding Sources

The authors acknowledge funding from the Hessen State Ministry of Higher Education, Research and the Arts, Germany, in the frame of the LOEWE project iNAPO. Annette Andrieu-Brunsen acknowledges funding from the European Research Council (ERC) under the European Union's Horizon 2020 research and innovation programme (grant agreement No 803758).

ACKNOWLEDGMENT

The authors cordially thank Prof. Bernd Stühn, Dr. Christina Lederle and Dr. Michael Appold for help with DLS measurements and discussion of the results, Lilia Proskurjakov for further end-functionalization experiments and Andreas Geißler for support with SEM measurements. The authors acknowledge funding from the Hessen State Ministry of Higher Education, Research and the Arts, Germany, in the frame of the LOEWE project iNAPO. Annette Andrieu-Brunsen acknowledges funding from the European Research Council (ERC) under the European Union's Horizon 2020 research and innovation programme (grant agreement No 803758).

REFERENCES

Uncategorized References

1. Deng, Y.; Wei, J.; Sun, Z.; Zhao, D., Large-pore ordered mesoporous materials templated from non-Pluronic amphiphilic block copolymers. *Chem. Soc. Rev.* **2013,** *42* (9), 4054-70.
2. Innocenzi, P.; Malfatti, L., Mesoporous thin films: properties and applications. *Chem. Soc. Rev.* **2013,** *42* (9), 4198-216.
3. Calvo, A.; Angelomé, P. C.; Sanchez, C.; Scherlis, D. A.; Williams, F. J.; Soler-Illia, G. J. A. A., Mesoporous Aminopropyl-Functionalized Hybrid Thin Films with Modulable Surface and Environment-Responsive Behavior. *Chem. Mater.* **2008,** *20*, 4661-4668.
4. Soler-Illia, G. J.; Azzaroni, O., Multifunctional hybrids by combining ordered mesoporous materials and macromolecular building blocks. *Chem. Soc. Rev.* **2011,** *40* (2), 1107-50.
5. Sun, M. H.; Huang, S. Z.; Chen, L. H.; Li, Y.; Yang, X. Y.; Yuan, Z. Y.; Su, B. L., Applications of hierarchically structured porous materials from energy storage and conversion, catalysis, photocatalysis, adsorption, separation, and sensing to biomedicine. *Chem. Soc. Rev.* **2016,** *45* (12), 3479-563.
6. Nisticò, R.; Scalarone, D.; Magnacca, G., Sol-gel chemistry, templating and spin-coating deposition: A combined approach to control in a simple way the porosity of inorganic thin films/coatings. *Microporous and Mesoporous Materials* **2017,** *248*, 18-29.
7. Nicole, L.; Boissiere, C.; Grosso, D.; Quach, A.; Sanchez, C., Mesostructured hybrid organic–inorganic thin films. *J. Mater. Chem.* **2005,** *15*, 3598-3627.
8. Hoffmann, F.; Cornelius, M.; Morell, J.; Froba, M., Silica-based mesoporous organic-inorganic hybrid materials. *Angew. Chem. Int. Ed. Engl.* **2006,** *45* (20), 3216-51.
9. Sanchez, C.; Boissiere, C.; Grosso, D.; Laberty, C.; Nicole, L., Design, Synthesis, and Properties of Inorganic and Hybrid Thin Films Having Periodically Organized Nanoporosity. *Chem. Mater.* **2008,** *20*, 682-737.
10. Stein, P.; Vrankovic, D.; Graczyk-Zajac, M.; Riedel, R.; Xu, B.-X., A Model for Diffusion and Immobilization of Lithium in SiOC Nanocomposite Anodes. *JOM* **2017,** *69* (9), 1524-1531.
11. Graczyk-Zajac, M.; Vrankovic, D.; Waleska, P.; Hess, C.; Sasikumar, P. V.; Lauterbach, S.; Kleebe, H.-J.; Sorarù, G. D., The Li-storage capacity of SiOC glasses with and without mixed silicon oxycarbide bonds. *Journal of Materials Chemistry A* **2018,** *6* (1), 93-103.
12. Zhulina, E. B.; Borisov, O. V., Theory of Block Polymer Micelles: Recent Advances and Current Challenges. *Macromolecules* **2012,** *45* (11), 4429-4440.
13. Kim, H.-C.; Park, S.-M.; Hinsberg, W. D., Block Copolymer Based Nanostructures: Materials, Processes, and Applications to Electronics. *Chemical Reviews* **2010,** *110* (1), 146-177.
14. Hayward, R. C.; Pochan, D. J., Tailored Assemblies of Block Copolymers in Solution: It Is All about the Process. *Macromolecules* **2010,** *43* (8), 3577-3584.
15. Brinker, C. J.; Scherer, G. W., *Sol-Gel Science - The Physics and Chemistry of Sol-Gel Processing*. Academic Press Inc. - an Imprint of Elsevier: San Diego, **1990**.
16. Raffa, P.; Wever, D. A.; Picchioni, F.; Broekhuis, A. A., Polymeric Surfactants: Synthesis, Properties, and Links to Applications. *Chem. Rev.* **2015,** *115* (16), 8504-63.
17. Bathfield, M.; Reboul, J.; Cacciaguerra, T.; Lacroix-Desmazes, P.; Gérardin, C., Thermosensitive and Drug-Loaded Ordered Mesoporous Silica: A Direct and Effective Synthesis Using PEO-b-PNIPAM Block Copolymers. *Chemistry of Materials* **2016,** *28* (10), 3374-3384.
18. Liu, J.; Bai, S.; Jin, Q.; Li, C.; Yang, Q., Enhanced thermostability of enzymes accommodated in thermo-responsive nanopores. *Chemical Science* **2012,** *3* (12).

19. Tom, J. C.; Appel, C.; Andrieu-Brunsen, A., Fabrication and in situ functionalisation of mesoporous silica films by the physical entrapment of functional and responsive block copolymer structuring agents. *Soft Matter* **2019,** *15* (40), 8077-8083.
20. Yang, H.; Coombs, N.; Sokolov, I.; Ozin, G. A., Free-standing and oriented mesoporous silica films grown at the air-water interface. *Nature* **1996,** *381*, 589-592.
21. Yang, H.; Kuperman, A.; Coombs, N.; Mamiche-Afara, S.; Ozin, G. A., Synthesis of oriented films of mesoporous silica on mica. *Nature* **1996,** *379*, 703-705.
22. Brinker, C. J.; Lu, Y.; Sellinger, A.; Fan, H., Evaporation-Induced Self-Assembly: Nanostructures Made Easy. *Adv. Mater.* **1999,** *11* (7), 579-585.
23. Lu, Y.; Fan, H.; Stump, A.; Ward, T. L.; Rieker, T.; Brinker, C. J., Aerosol-assisted selfassembly of mesostructured spherical nanoparticles. *Nature* **1999,** *398*, 223-226.
24. Wei, J.; Sun, Z.; Luo, W.; Li, Y.; Elzatahry, A. A.; Al-Enizi, A. M.; Deng, Y.; Zhao, D., New Insight into the Synthesis of Large-Pore Ordered Mesoporous Materials. *J. Am. Chem. Soc.* **2017,** *139* (5), 1706-1713.
25. De Paz-Simon, H.; Chemtob, A.; Croutxé-Barghorn, C.; Rigolet, S.; Michelin, L.; Vidal, L.; Lebeau, B., Periodic Mesostructured Silica Films Made Simple Using UV Light. *The Journal of Physical Chemistry C* **2014,** *118* (9), 4959-4966.
26. Cagnol, F.; Grosso, D.; Sanchez, C., A general one-pot process leading to highly functionalised ordered mesoporous silica films. *Chem. Commun.* **2004,** (15), 1742-3.
27. Brilmayer, R.; Hess, C.; Andrieu-Brunsen, A., Influence of Chain Architecture on Nanopore Accessibility in Polyelectrolyte Block-Co-Oligomer Functionalized Mesopores. *Small* **2019,** *15* (41), 1902710.
28. Elbert, J.; Krohm, F.; Rüttiger, C.; Kienle, S.; Didzoleit, H.; Balzer, B. N.; Hugel, T.; Stühn, B.; Gallei, M.; Brunsen, A., Polymer-Modified Mesoporous Silica Thin Films for Redox-Mediated Selective Membrane Gating. *Advanced Functional Materials* **2014,** *24* (11), 1591-1601.
29. Silies, L.; Andrieu-Brunsen, A., Programming Ionic Pore Accessibility in Zwitterionic Polymer Modified Nanopores. *Langmuir* **2017**.
30. Zhu, Z.; Wang, D.; Tian, Y.; Jiang, L., Ion/Molecule Transportation in Nanopores and Nanochannels: From Critical Principles to Diverse Functions. *Journal of the American Chemical Society* **2019,** *141* (22), 8658-8669.
31. Fu, L.; Zhai, J., Biomimetic stimuli-responsive nanochannels and their applications. *ELECTROPHORESIS* **2019,** *40* (16-17), 2058-2074.
32. Pérez-Mitta, G.; Toimil-Molares, M. E.; Trautmann, C.; Marmisollé, W. A.; Azzaroni, O., Molecular Design of Solid-State Nanopores: Fundamental Concepts and Applications. *Advanced Materials* **2019,** *31* (37), 1901483.
33. Powell, M. R.; Cleary, L.; Davenport, M.; Shea, K. J.; Siwy, Z. S., Electric-field-induced wetting and dewetting in single hydrophobic nanopores. *nature nanotechnology* **2011,** *6* (12), 798-802.
34. Siwy, Z. S.; Howorka, S., Engineered voltage-responsive nanopores. *Chem. Soc. Rev.* **2010,** *39* (3), 1115-32.
35. Tom, J.; Brilmayer, R.; Schmidt, J.; Andrieu-Brunsen, A., Optimisation of Surface-Initiated Photoiniferter-Mediated Polymerisation under Confinement, and the Formation of Block Copolymers in Mesoporous Films. *Polymers* **2017,** *9* (10), 539.

36. Krohm, F.; Kind, J.; Savka, R.; Alcaraz Janßen, M.; Herold, D.; Plenio, H.; Thiele, C. M.; Andrieu-Brunsen, A., Photochromic spiropyran- and spirooxazine-homopolymers in mesoporous thin films by surface initiated ROMP. *J. Mater. Chem. C* **2016,** *4* (18), 4067-4076.
37. Silies, L.; Gonzalez Solveyra, E.; Szleifer, I.; Andrieu-Brunsen, A., Insights into the Role of Counterions on Polyelectrolyte-Modified Nanopore Accessibility. *Langmuir* **2018,** *34* (20), 5943-5953.
38. Yang, P.; Pageni, P.; Kabir, M. P.; Zhu, T.; Tang, C., Metallocene-Containing Homopolymers and Heterobimetallic Block Copolymers via Photoinduced RAFT Polymerization. *ACS Macro Letters* **2016,** *5* (11), 1293-1300.
39. Hardy, C. G.; Ren, L.; Zhang, J.; Tang, C., Side-Chain Metallocene-Containing Polymers by Living and Controlled Polymerizations. *Israel Journal of Chemistry* **2012,** *52* (3-4), 230-245.
40. Gallei, M.; Rüttiger, C., Recent Trends in Metallopolymer Design: Redox-Controlled Surfaces, Porous Membranes, and Switchable Optical Materials Using Ferrocene-Containing Polymers. *Chemistry* **2018,** *24* (40), 10006-10021.
41. Elbert, J.; Gallei, M.; Rüttiger, C.; Brunsen, A.; Didzoleit, H.; Stühn, B.; Rehahn, M., Ferrocene Polymers for Switchable Surface Wettability. *Organometallics* **2013,** *32* (20), 5873-5878.
42. Rüttiger, C.; Mehlhase, S.; Vowinkel, S.; Cherkashinin, G.; Liu, N.; Dietz, C.; Stark, R. W.; Biesalski, M.; Gallei, M., Redox-mediated flux control in functional paper. *Polymer* **2016,** *98*, 429-436.
43. Dubois, C.; Herzog, N.; Rüttiger, C.; Geissler, A.; Grange, E.; Kunz, U.; Kleebe, H. J.; Biesalski, M.; Meckel, T.; Gutmann, T.; Gallei, M.; Andrieu-Brunsen, A., Fluid Flow Programming in Paper-Derived Silica-Polymer Hybrids. *Langmuir* **2017,** *33* (1), 332-339.
44. Scheid, D.; Lederle, C.; Vowinkel, S.; Schäfer, C. G.; Stühn, B.; Gallei, M., Redox- and mechano-chromic response of metallopolymer-based elastomeric colloidal crystal films. *Journal of Materials Chemistry C* **2014,** *2* (14), 2583-2590.
45. Scheid, D.; von der Lühe, M.; Gallei, M., Synthesis of Breathing Metallopolymer Hollow Spheres for Redox-Controlled Release. *Macromolecular Rapid Communications* **2016,** *37* (19), 1573-1580.
46. Staff, R. H.; Gallei, M.; Mazurowski, M.; Rehahn, M.; Berger, R.; Landfester, K.; Crespy, D., Patchy Nanocapsules of Poly(vinylferrocene)-Based Block Copolymers for Redox-Responsive Release. *ACS Nano* **2012,** *6* (10), 9042-9049.
47. Kloninger, C.; Rehahn, M., 1,1-Dimethylsilacyclobutane-Mediated Living Anionic Block Copolymerization of [1]Dimethylsilaferrocenophane and Methyl Methacrylate. *Macromolecules* **2004,** *37* (5), 1720-1727.
48. Schmidt, B. V. K. J.; Elbert, J.; Scheid, D.; Hawker, C. J.; Klinger, D.; Gallei, M., Metallopolymer-Based Shape Anisotropic Nanoparticles. *ACS Macro Letters* **2015,** *4* (7), 731-735.
49. Shen, L.; Wang, H.; Guerin, G.; Wu, C.; Manners, I.; Winnik, M. A., A Micellar Sphere-to-Cylinder Transition of Poly(ferrocenyldimethylsilane-b-2-vinylpyridine) in a Selective Solvent Driven by Crystallization. *Macromolecules* **2008,** *41* (12), 4380-4389.
50. Wang, H.; Winnik, M. A.; Manners, I., Synthesis and Self-Assembly of Poly(ferrocenyldimethylsilane-b-2-vinylpyridine) Diblock Copolymers. *Macromolecules* **2007,** *40*, 3784-3789.

51. Wang, H.; Lin, W.; Fritz, K. P.; Scholes, G. D.; Winnik, M. A.; Manners, I., Cylindric Block Co-Micelles with Spatially Selective Functionalization by Nanoparticles. *J. Am. Chem. Soc.* **2007,** *129*, 12924-12925.
52. Shin, W.-J.; Kim, J.-Y.; Cho, G.; Lee, J.-S., Highly selective incorporation of SiO2nanoparticles in PS-b-P2VP block copolymers by quaternization. *Journal of Materials Chemistry* **2009,** *19* (39), 7322-7325.
53. Lim, C.-S.; Seok, S. I.; Im, S. H., Synthesis of uniform PS-b-P2VP nanoparticles via reprecipitation and their use as sacrificial templates for inorganic hollow nanoparticles. *Journal of Materials Chemistry* **2012,** *22* (18), 8772-8774.
54. Calvo, A.; Yameen, B.; Williams, F. J.; Soler-Illia, G. J. A. A.; Azzaroni, O., Mesoporous Films and Polymer Brushes Helping Each Other To Modulate Ionic Transport in Nanoconfined Environments. An Interesting Example of Synergism in Functional Hybrid Assemblies. *J. Am. Chem. Soc.* **2009,** *131*, 10866-10868.
55. Rosenholm, J. M.; Czuryszkiewicz, T.; Kleitz, F.; Rosenholm, J. B.; Lindén, M., On the Nature of the Broensted Acidic Groups on Native and Functionalized Mesoporous Siliceous SBA-15 as Studied by Benzylamine Adsorption from Solution. *Langmuir* **2007,** *23*, 4315-4323.
56. Sulpizi, M.; Gaigeot, M. P.; Sprik, M., The Silica-Water Interface: How the Silanols Determine the Surface Acidity and Modulate the Water Properties. *J. Chem. Theory Comput.* **2012,** *8* (3), 1037-47.
57. Tantavichet, N.; Pritzker, M. D.; Burns, C. M., Proton Uptake by Poly(2-vinylpyridine) Coatings. *Journal of Applied Polymer Science* **2001,** *81* (6), 1493-1497.
58. Brunsen, A.; Calvo, A.; Williams, F. J.; Soler-Illia, G. J.; Azzaroni, O., Manipulation of molecular transport into mesoporous silica thin films by the infiltration of polyelectrolytes. *Langmuir* **2011,** *27* (8), 4328-33.
59. Andrieu-Brunsen, A.; Micoureau, S.; Tagliazucchi, M.; Szleifer, I.; Azzaroni, O.; Soler-Illia, G. J. A. A., Mesoporous Hybrid Thin Film Membranes with PMETAC@Silica Architectures: Controlling Ionic Gating through the Tuning of Polyelectrolyte Density. *Chemistry of Materials* **2015,** *27* (3), 808-821.
60. Silies, L.; Didzoleit, H.; Hess, C.; Stühn, B.; Andrieu-Brunsen, A., Mesoporous Thin Films, Zwitterionic Monomers, and Iniferter-Initiated Polymerization: Polymerization in a Confined Space. *Chemistry of Materials* **2015,** *27* (6), 1971-1981.
61. Herzog, N.; Kind, J.; Hess, C.; Andrieu-Brunsen, A., Surface plasmon & visible light for polymer functionalization of mesopores and manipulation of ionic permselectivity. *Chem. Commun.* **2015,** *51* (58), 11697-700.
62. Masson, G.; Beyer, P.; Cyr, P. W.; Lough, A. J.; Manners, I., Synthesis and Reversible Redox Properties of an Electron-Rich Polyferrocenylsilane with tert-Butyl Substituents on the Cyclopentadienyl Ligands. *Macromolecules* **2006,** *39* (11), 3720-3730.
63. Kulbaba, K.; MacLachlan, M. J.; Evans, C. E. B.; Manners, I., Organometallic Gels: Characterization and Electrochemical Studies of Swellable, Thermally Crosslinked Poly(ferrocenylsilane)s. *Macromolecular Chemistry and Physics* **2001,** *202* (9), 1768-1775.
64. Cyr, P. W.; Tzolov, M.; Manners, I.; Sargent, E. H., Photooxidation and Photoconductivity of Polyferrocenylsilane Thin Films. *Macromolecular Chemistry and Physics* **2003,** *204* (7), 915-921.
65. Karman, C.; Vilà, N.; Walcarius, A., Amplified Charge Transfer for Anionic Redox Probes through Oriented Mesoporous Silica Thin Films. *Chem. Electro. Chem.* **2016,** *3* (12), 2130-2137.

66. Tagliazucchi, M.; Azzaroni, O.; Szleifer, I., Responsive Polymers End-Tethered in Solid-State Nanochannels: When Nanoconfinement Really Matters. *J. Am. Chem. Soc.* **2010,** *132*, 12404-12411.

ToC-Graphic:

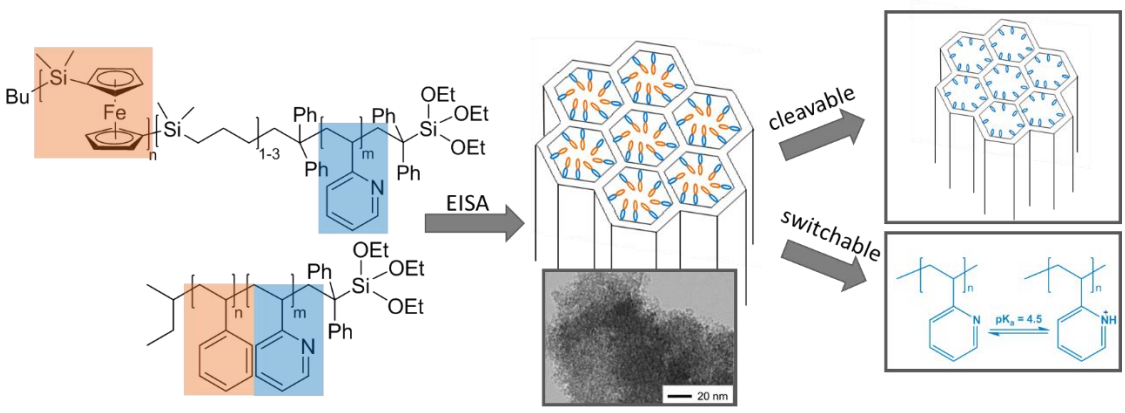
Bu
Si
Fe
n
Si
1-3
Ph
Ph
m
Ph
Ph
N
OEt
OEt
Si
OEt
EISA
n
m
Ph
OEt
Si
OEt
Ph
N
20 nm
cleavable
switchable
n
N
pK$_a$ = 4.5
n
NH